PFC/JA-94-014

# Scaling of Plasma Parameters in the SOL and Divertor for Alcator C-Mod

B. LaBombard, D. Jablonski,
B. Lipschultz, G.M. McCracken, J. Goetz

Plasma Fusion Center
Massachusetts Institute of Technology
Cambridge, MA 02139

June 1994

Submitted to Journal of Nuclear Materials.

This work was supported by the U. S. Department of Energy Contract No. DE-AC02-78ET51013. Reproduction, translation, publication, use and disposal, in whole or in part by or for the United States government is permitted.

# Scaling of Plasma Parameters in the SOL and Divertor for Alcator C-Mod

**B. LaBombard, D. Jablonski, B. Lipschultz, G. McCracken, J. Goetz**

Plasma Fusion Center
Massachusetts Institute of Technology
Cambridge, MA 02139, USA

A fast-scanning Langmuir probe and an array of divertor Langmuir probes are used to characterize the cross-field heat transport ($\chi_\perp$) and to compare plasma conditions 'upstream' along a magnetic flux tube to conditions at the divertor. Three distinct regimes are found which depend on the power into the SOL and the edge plasma density: (1) a sheath-limited conduction regime where the divertor target temperature and density is similar to the values upstream, (2) a high-recycling regime where plasma pressure is approximately constant along field lines while $n_e$ is high and $T_e$ is low at the divertor and (3) a detached divertor regime where $n_e$ and $T_e$ collapse near the divertor strike points. The scaling between regimes (1) and (2) can be described by a transport model that includes anomalous cross-field heat transport ($0.25 < \chi_\perp < 0.5$ m$^2$ s$^{-1}$), sheath conduction, and classical parallel electron conduction.

## 1. Introduction

The current understanding of edge plasma and divertor physics must be greatly expanded in order to design a high heat flux divertor for fusion reactors such as ITER with confidence. One key to understanding divertor physics is the scaling of edge with central plasma conditions and the identification of principal energy loss and transport mechanisms over a wide range of plasma regimes. Particularly important are the 'dissipative divertor' regimes which are currently envisioned to solve ITER's high heat flux problem [1].

Alcator C-Mod is a unique facility to explore divertor and edge physics phenomena at high magnetic field ($B \leq 9$ tesla), high SOL power density, ($q_{// sol} >$ 200 MW $m^{-2}$) and high divertor plasma density ($n_{div} > 5 \times 10^{20}$ $m^{-3}$) in a shaped divertor geometry and with metal (Mo) divertor and first-wall [2,3]. This paper reports upon edge plasma measurements and a simple plasma transport scaling analysis from the first run campaign (1993) of Alcator C-Mod.

Section 2 describes the experimental arrangement for this study which principally employed a divertor Langmuir probe array and a fast-scanning Langmuir probe. Section 3 presents results in two parts: measurements and transport analysis of plasma profiles across the magnetic field and measurements and transport analysis of density and temperature profiles along the magnetic field. Section 4 summarizes the key findings in this study.

## 2. Experiment

The present experiments were conducted in ohmically heated, diverted deuterium plasmas with central conditions of $B_T = 5$ tesla, $600 < I_p < 850$ kA, line-averaged density $0.5 < \bar{n}_e < 1.8 \times 10^{20}$ $m^{-3}$, and vertical elongation of 1.6. For the restricted set of discharges studied here, core radiation was 45% of the ohmic input power, jumping to 70% during divertor detachment [4]. The

resultant average power flux crossing the last closed flux surface was in the range of 25 to 100 kW $m^{-2}$. The geometry of the divertor and the arrangement of probe diagnostics is shown in Fig. (1).

Molybdenum probes are mounted on both the inner and outer divertor plates at 16 poloidal locations. Most of the probes in the array are designed for high heat-flux handling and have collection areas that are flush with the divertor surface. Probes at outer divertor locations 3, 7, and 9 project 0.5 mm beyond the surface of the divertor, presenting a domed surface to the plasma flux. Unlike the 'flush' probes, the 'domed' probes project a well defined area along the magnetic field lines and avoid the problems associated with the interpretation of probe characteristics at small oblique field line angles [5]. Data from the domed probe at position 7 on the outer divertor was used for the present studies.

A fast-scanning Langmuir probe is used to record plasma profiles upstream above the entrance of the divertor. The probe consists of a 15 mm diameter molybdenum body with four Langmuir probe elements. The probe elements are positioned along the four vertices of a pyramid. This arrangement allows the probes to have directional sensitivity (along and across B) and to maintain a field line grazing angle of about 20 degrees. The probe has a peak velocity of about 2 m $sec^{-1}$ and has been routinely used to record profiles up to the last closed flux surface (LCFS). Densities and temperatures along the probe's trajectory are obtained by fitting positive and negative-going I-V characteristics generated by a 500 Hz voltage sweep. Except in cases when the probe was overheated, densities and temperatures recorded during probe retraction are found to retrace the values obtained during insertion.

Owing to intermittent electrical shorts, only one probe element was able to record reliable data over all the discharges in this study. Because this probe element faces toward the divertor along field lines, it does exhibit shadowing

effects when the connection length from the probe to the divertor is under a few meters. To avoid this interpretation problem, the present analysis is restricted to data collected by the probe when the connection length was at least 5 meters.

Data from both the divertor probe array and the fast-scanning probe is mapped onto magnetic flux surfaces reconstructed from magnetic measurements [6] and the EFIT plasma equilibrium code [7]. Flux surfaces in the scrape-off layer are labeled by the coordinate, $\rho$, which is defined as the distance in major radius from the last-closed flux surface at the outboard midplane.

## 3. Results

### 3.1 *SOL profiles*

The shape of the cross-field density and temperature profiles recorded by the scanning probe shows some variation from discharge to discharge but generally exhibits an exponential dependence on $\rho$. The uncertainty in $\rho$ from magnetic reconstruction is estimated to be a few millimeters.

Figures 2, and 3 show the density and electron temperature at the LCFS ($n_{sep}$, $T_{sep}$) and the pressure e-folding length at the outside midplane ($\lambda_p = \frac{\lambda_n \lambda_T}{\lambda_n + \lambda_T}$) that results from fitting a single exponential function of $\rho$ to the measured density and temperature profiles. Discharges represented by these 41 points were selected based on the quality of the probe data (no overheating, good bias range on I-V trace, etc.) and by the quality of the central plasma (disruption free, steady-state portion of discharge, no impurity injection events).

For the discharges studied, $n_{sep}$ scales roughly in proportion to the central line-averaged density, $\bar{n}_e$. However, $T_{sep}$ and $\lambda_p$ appear to be best represented as functions of $\bar{n}_e/I_p$, the line-averaged density divided by the plasma current. This relationship appears to hold for a factor 1.5 variation in $\bar{n}_e$ at fixed current and a factor of 1.4 variation in $I_p$ at fixed central density. An empirical scaling of edge

plasma conditions with $\bar{n}_e / I_p$ has been seen before in other tokamaks [8,9,10], and has been indirectly evidenced in the overall scaling of tokamak edge phenomena with $\bar{n}_e/I_p$ such as in density limits, MARFEs [11] and more recently, divertor detachment [3].

The detached divertor regime appears in Alcator C-Mod as an abrupt decrease in the ion current to divertor probes near the inner and outer strike points and a rearrangement in the divertor radiation [2,3]. Data points taken during detached divertor operation (shown as ◆ symbols in Figs. 2 and 3) indicate that the scrape-off layer conditions scale in a way that is a simple extension to the normal, attached divertor discharges. The linear relationship between $n_{sep}$ and $\bar{n}_e$ does however appear to be violated during divertor detachment at the highest densities.

### 3.2 $\perp$ *Transport analysis*

Measurements of input power, core radiation, and plasma conditions at the LCFS can be combined to estimate the perpendicular heat diffusivity in the SOL. Assuming that $\chi_\perp^i \cong \chi_\perp^e$, the cross field heat flux can be written as the sum of conduction and convection terms,

$$q_\perp = q_\perp^i + q_\perp^e = -\chi_\perp n \nabla_\perp (T_i + T_e) + \frac{5}{2} (T_i + T_e) D_\perp \nabla_\perp n \,. \qquad (1)$$

If one further assumes (for convenience) that particle and heat diffusivity satisfy $D_\perp \cong \frac{2}{5} \chi_\perp$ and that $T_i \approx T_e$ then

$$q_\perp \cong -4 \chi_\perp \nabla_\perp n T_e \qquad (2)$$

so that $\chi_\perp$ can be computed from the net power crossing the LCFS ($P_{OH}$ - $P_{Rad}$), the LCFS area ($A_{sep}$), and measurements of density, electron temperature, and pressure e-folding length at the LCFS from

$$\chi_{\perp} \cong \frac{P_{OH} - P_{Rad}}{4\, A_{sep}\, n_{sep} T_{sep} \left\langle 1/\lambda_p \right\rangle}, \qquad (3)$$

where $\left\langle 1/\lambda_p \right\rangle$ is the average value of $1/\lambda_p$ over the LCFS.

Figure 4 plots $\chi_{\perp}$ from Eq. (3) versus $\bar{n}_e/I_p$ for the test discharges. For a given value of $\bar{n}_e$ and $I_p$, the density, temperature, and pressure e-folding length at the separatrix is obtained from the straight line fits shown in Figs. (2) and (3). $P_{OH}$ and $A_{sep}$ are determined separately for each discharge and $P_{Rad}$ is determined from bolometry for these discharges to be 0.45 $P_{OH}$ for attached divertor conditions (◇) and 0.7 $P_{OH}$ for detached divertor conditions (◆).

Values for $\chi_{\perp}$ computed by this method are in the range of 0.25 to 0.5 $m^2$ $s^{-1}$. For comparison, $\frac{T_e}{16\,B}$ yields Bohm diffusion values of 0.19 to 0.38 $m^2$ $s^{-1}$ although, in contrast, $\chi_{\perp}$ appears to scale inversely with $T_e$ from these data. The discontinuity suggested by the separate grouping of detached divertor points in Fig. (4) is suggestive that $\chi_{\perp}$ changes markedly during detachement. This may however be the result of specifying a step change in $P_{Rad}$ for the detach discharges in this data set. It remains to be seen if this trend continues with a more complete data set and with better power accounting.

Examining the assumption that $D_{\perp} \cong \frac{2}{5}\chi_{\perp}$, we see that $D_{\perp}$ must be in the range of 0.1 to 0.2 $m^2$ $s^{-1}$ to validate the transport analysis. This range of $D_{\perp}$ is found to compare favorably with edge impurity diffusion coefficients from laser blow-off experiments [12] and from diffusion coefficients deduced from $H\alpha$ light inside the last closed flux surface [13] combined with the measured values of $\lambda_n$ at the separatrix.

3.3 // *Density and Temperature Gradients*

Both probe systems were operated in these discharges to compare plasma conditions at the divertor surface to conditions 'upstream', at the scanning-probe location. Our goal in these experiments was to look for gradients in density and temperature along **B** and to characterize the scaling of these gradients with central plasma conditions. The task was complicated by the fact that the magnetic equilibrium and separatrix strike points varied somewhat from discharge to discharge as central plasma conditions were adjusted. A jitter in separatrix position appears as scatter in the probe measurements for discharges that would otherwise be identical. Still, as long as the jitter is not correlated with systematic variations in central plasma conditions, one can treat the scatter in the probe measurements as an additional 'noise', and look for systematic scalings.

To facilitate the comparison, we focus attention on density and temperature measurements from probe 7 on the outer divertor and corresponding measurements from the scanning probe on the same magnetic flux surface. The $\rho$ of the magnetic 'flux tube' intercepting probe 7 varied randomly between 1 to 4 mm for these discharges. Figure 5 displays the simultaneous measurements versus $\bar{n}_e/I_p$, grouping the data into three regimes:

1 - At low density and high current (or input power), $\bar{n}_e/I_p < 1.3 \times 10^{14}$ $A^{-1}m^{-3}$, the electron temperature is virtually constant along the magnetic field lines. Pressure is also constant along **B** and the divertor sheath appears to support all of the temperature drop.

2 - At moderate density divided by plasma current, $1.3 < \bar{n}_e/I_p < 1.8 \times 10^{14}$ $A^{-1}m^{-3}$, a 'high recycling' divertor condition arises, namely, the electron temperature falls at the divertor plate relative to 'upstream' while the density rises there so as to keep pressure approximately constant along **B**. A temperature gradient arises along the field line presumably because parallel electron thermal

conduction is poorer at lower temperatures ($\kappa \propto T^{5/2}$), while the divertor sheath temperature is lower since it conducts heat more readily at higher densities. In this regime, the density at the divertor plate shows a clear nonlinear scaling with core density and is found to routinely exceed the central line-averaged density.

3 - At the highest densities and lowest currents, $\bar{n}_e/I_p > 1.8 \times 10^{14}$ $A^{-1}m^{-3}$, the divertor plasma 'detaches' from the divertor plate. Both the divertor electron temperature and the plasma density are very low in this regime, violating constant pressure along B. Note that a small change in $\bar{n}_e$ and/or $I_p$ can lead to a factor of 10 or more reduction in the density at the divertor plate. This is why divertor detachment appears coincidentally with a large change in the ion currents collected by the divertor probes.

### 3.4 // *Transport analysis*

A quantitative comparison can be made between the experimental observations and a standard heat transport model that balances anomalous perpendicular transport with classical electron parallel conduction, sheath-limited heat flow, and edge radiation.

Conservation of energy in this model requires

$$\nabla_{//} \cdot q_{//} + \nabla_{\perp} \cdot q_{\perp} + Q_{Rad} = 0 \qquad (4)$$

while $q_{//}$ in the bulk plasma is $q_{//} \cong -\frac{2}{7} \kappa_0 \nabla_{//} T^{7/2}$ and at the sheath is

$$q_{//}\Big|_{sheath} = e \gamma n_d T_d^{3/2} \sqrt{\frac{2e}{m_i}} \quad . \qquad (5)$$

Here, $\kappa_0$ is $2.8 \times 10^3$ W $m^{-1}$ $eV^{-7/2}$, e is $1.6 \times 10^{-19}$ J $eV^{-1}$, $\gamma$ is the sheath heat transfer coefficient, and subscripts 'd' refer to conditions at the divertor plate.

Now consider that the measurements were made in a magnetic flux tube of length $S_d$, extending from the symmetry point, S=0, to the divertor surface, $S=S_d$. Integrating Eq. (4) over the length of the flux tube,

$$q_{//}\Big|_{sheath} = -\langle \nabla_\perp \cdot q_\perp \rangle S'_d - \int_0^{S_d} Q_{Rad}\, \partial S = -(1-f_{Rad})\langle \nabla_\perp \cdot q_\perp \rangle S'_d , \quad (6)$$

where $f_{Rad}$ is defined as the fraction of total power into the flux tube that is radiated rather than conducted to the sheath and $\langle \nabla_\perp \cdot q_\perp \rangle$ represents an average value along the flux tube's length over a distance $S'_d$. $S'_d$ is loosely defined as the length of the flux tube outside the divertor region. This formulation accounts for the fact that $\langle \nabla_\perp \cdot q_\perp \rangle$ is smaller in the divertor since the core plasma - SOL plasma interface changes to a private flux - common flux SOL plasma interface there. Given that $q_\perp$ follows Eq. (2), this quantity can be approximated for a flux tube at position $\rho$ as

$$\langle \nabla_\perp \cdot q_\perp \rangle \cong -\left\langle \frac{1}{\lambda_p} \right\rangle \frac{P_{OH} - P_{Rad}}{A_{sep}} e^{-\rho/\lambda_p} \quad (7)$$

which replaces the average along the flux tube length $S'_d$ with the average over the LCFS. Requiring that stagnation pressure be constant along B (no detachment) so that

$$2\, n\, T\, (1+M^2) = 2\, n_{sep}\, T_{sep}\, e^{-\rho/\lambda_p}, \quad (8)$$

yields an expression for the divertor temperature,

$$T_d^{1/2} = \left\langle \frac{1}{\lambda_p} \right\rangle \frac{(P_{OH} - P_{Rad})\,(1-f_{Rad})\,2\,S'_d}{e\, A_{sep}\, n_{sep} T_{sep}\, \gamma \sqrt{\frac{2e}{m_i}}} . \quad (9)$$

The temperature upstream from the divertor can be obtained from integrating Eq. (4) twice and by assuming a model profile for the distribution of radiation along the length of the flux tube. Assuming that the radiation emissivity decreases exponentially away from the divertor with a parallel decay length of $\lambda_{Rad}$,

$$Q_{Rad} = Q_0\, e^{(S - S_d)/\lambda_{Rad}}, \quad (10)$$

the upstream temperature is

$$T^{7/2} = T_d^{7/2} + \frac{7}{2K_0}\left\langle\frac{1}{\lambda_p}\right\rangle\frac{P_{OH}-P_{Rad}}{A_{sep}}e^{-\rho/\lambda_p}$$

$$\times\left\{\frac{S'^2_d-S^2}{2}+(S_d-S'_d)S'_d-\frac{f_{Rad}\,S'_d\,\lambda_{Rad}}{1-e^{-S_d/\lambda_{Rad}}}\left[1+\frac{S-S_d}{\lambda_{Rad}}e^{-S_d/\lambda_{Rad}}-e^{(S-S_d)/\lambda_{Rad}}\right]\right\} \tag{11}$$

This expression is valid for $S < S'_d$. The scanning probe was at the location $S/S_d \approx 0.5$ in the set of discharges studied here.

3.5 *Comparison with Experiment*

The curved lines drawn over the data points in Fig. 5 show the corresponding scaling of divertor temperatures and densities predicted by Eqs. (8), and (9). The magnitude and scaling is in good agreement with experiment. The curves where generated from the following procedure: Measurements of $P_{OH}$, $P_{Rad}$, $A_{sep}$, $S_d$, S, and $\rho$ were taken from each discharge. Values for $n_{sep}$, $T_{sep}$, and $\langle 1/\lambda_p \rangle$ were determined from the straight line fits in Figs. (2) and (3) at the corresponding $\bar{n}_e$ and $I_p$ of each discharge. The parameters $\gamma$, and $f_{Rad}$ where assumed to be constant for all discharges and adjusted so that the temperature predicted from Eq. (9) agreed with experimental values, particularly in the high recycling regime. The resultant set of theoretical data points was plotted versus $\bar{n}_e/I_p$ and smooth spline curves were fitted through these points. These spline curves are plotted over the actually measured data points in Fig. (5).

Values of $\gamma \approx 6.7$ and $f_{Rad} \approx 0.80$ with $S'_d/S_d \approx 0.83$ (estimated from geometry) resulted in the best fit to the data. These values are consistent with the magnitude of standard sheath heat-transmission coefficients and bolometer measurements which show that approximately 80% of the power into the SOL is radiated in the divertor region in these discharges [4].

In contrast, the magnitude of the upstream temperatures predicted by Eq. (11) does not show good agreement with the fast-scanning probe data. Although Eq. (11) predicts that the upstream temperature is indeed insensitive to the variation in discharge conditions (similar to the experimental result), typical values range between 30 to 40 eV. These are much higher than in the experiment and are quite insensitive to the assumed values of $\lambda_{Rad}/S_d$ and $S'_d/S_d$. A similar inconsistency in the SOL $T_e$ has been identified using the EDGE2D code, although these simulations do not yet include edge impurity radiation. A number of possible explanations for this discrepancy are currently under investigation including: effect of parallel convected heat fluxes, $T_i >> T_e$ in the SOL, and divertor radiation inside the LCFS.

A comparison of the scaling of the theoretical temperatures and densities with the observations is perhaps more important than a comparison of the absolute values. In this respect, Fig. (5) shows that the transport model agrees well in matching the observed scaling. Eqs.(8), (9), and (11) show us algebraically why the edge temperatures and densities scale as observed. For example, the divertor temperature is seen from Eq.(9) to be a strong function of $\langle 1/\lambda_p \rangle$ and $P_{OH}/n_{sep}$, both of which depend on $I_p/\bar{n}_e$. Whereas the temperature upstream is seen to be weakly dependent on $\bar{n}_e$ or $I_p$. Since the three observed transport regimes are defined according to the conditions at the divertor plate, it is not surprising then that they differentiate according the to empirical parameter $\bar{n}_e/I_p$ in these discharges.

## 4. Conclusions

Measurements in the edge plasma of Alcator C-Mod indicate that the perpendicular heat diffusivity at the last closed flux surface is in the range of 0.25 to 0.5 $m^2\ s^{-1}$ for plasma currents, $600 < I_p < 850$ kA, central line-averaged

densities, $0.5 < \bar{n}_e < 1.8 \times 10^{20}$ $m^{-3}$, and with ohmic heating. The density at the separatrix is found to scale approximately linear with the central density while the separatrix temperature is found to decrease monotonically as a function of $\bar{n}_e/I_p$. Density and temperature e-folding lengths scale together, increasing monotonically as a function of $\bar{n}_e/I_p$.

Measurements of density and temperature gradients along magnetic field lines indicate three distinct transport regimes: (1) a sheath-limited conduction regime at high SOL power and low plasma density where the density and temperature is nearly constant along a magnetic field line, (2) a 'high-recycling' regime at moderate densities where parallel temperature and density gradients are clearly established, and (3) a 'detached divertor' regime at the highest densities where the density, temperature, and heat flux at the divertor plate fall dramatically and plasma pressure is no longer constant along a field line.

The scaling and magnitude of conditions at the divertor plate in the first two regimes is found to be quantitatively consistent with a model that balances parallel heat transport by sheath conduction with the measured level of anomalous perpendicular heat transport and radiation. While the scaling of conditions 'upstream' from the divertor is consistent with a classical parallel electron conduction model, the magnitude of the electron temperature predicted by this model is higher than in the experiment. Effects which are not included in this model such as convected heat fluxes, $T_i >> T_e$ in the SOL, and divertor radiation inside the LCFS are currently being investigated.

## Acknowledgment

Special thanks are extended to I. H. Hutchinson for valuable comments and suggestions. This work was supported by the US Department of Energy Contract No. DE-AC02-78ET51013.

## References


[1] Janeschitz and Borass, Nucl. Fusion, to be published.

[2] I. H. Hutchinson et al., Physics of Fluids B, (1994) to be published.

[3] B. Lipschultz, J. Goetz, B. LaBombard et al, J. Nucl. Mater., this conference.

[4] J. Goetz et al., J. Nucl. Mater., this conference.

[5] G.F. Matthews, S.J. Fielding, G.M. McCracken et al., Plasma Phys. Control. Fusion **32** (1990) 1301.

[6] R.S. Granetz, I.H. Hutchinson, J. Gerolamo, et al., Rev. Sci. Instrum. **61** (1990) 2967.

[7] L.L. Lao, H. St. John, R.D. Stambaugh et al., Nucl. Fusion **25** (1985) 1611.

[8] V. Pericoli-Ridolfini, Plasma Phys. Controll. Fusion **27** (1985) 493.

[9] B LaBombard, Poloidal Asymmetries in the Limiter Shadow Plasma of the Alcator C Tokamak, M.I.T. Plasma Fusion Center report PFC/RR-86-6 (1986).

[10] S.K. Erents, J.A. Tagle, G.M. McCracken et al., Nucl. Fusion **28** (1988) 1209.

[11] B. Lipschultz, J. Nucl. Mater. 145-147 (1987) 15.

[12] M. Graf et al., Rev. Sci. Instrum., to be published

[13] C. Kurz, B. Lipschultz, G.M. McCracken et al., J. Nucl. Mater., this conference.

**Figure Captions**

Fig. 1 - Cross section of Alcator C-Mod showing the divertor geometry and probe locations. Data from the outer divertor probe array at location 7 is used in combination with scanning probe data to study the dependence of density and temperature variations along a magnetic flux tube with central plasma conditions.

Fig. 2 - Density at the last closed flux surface plotted as a function of central line-averaged density. Data points include a plasma current variation of $600 < I_p < 850$ kA at fixed densities. ($\diamond$ = discharges with attached divertor plasma; $\blacklozenge$ = discharges with detached divertor plasma)

Fig. 3 - (a) Electron temperature at the last closed flux surface and (b) Plasma pressure e-folding length ($\lambda_p = \frac{\lambda_n \lambda_T}{\lambda_n + \lambda_T}$) plotted as a function of central line-averaged density normalized to plasma current. Data points include a factor 1.5 variation in $\bar{n}_e$ at fixed current and a factor of 1.4 variation in $I_p$ at fixed central density. Density and temperature e-folding lengths are found to scale similarly with $\lambda_n \approx 1.5\,\lambda_p$ and $\lambda_T \approx 2.6\,\lambda_p$. ($\diamond$ = discharges with attached divertor plasma; $\blacklozenge$ = discharges with detached divertor plasma)

Fig. 4 - $\chi_\perp$ computed from Eq. (3) for the same discharges as in Figs. 2 and 3.

Fig. 5 - (a) Electron temperature and (b) plasma density simultaneously recorded by outer divertor probe 7 (symbols $\blacktriangle$ and $\blacksquare$) and the fast-scanning probe (symbols $\diamond$ and $\circ$) on the same magnetic flux surface. The solid lines indicate the theoretical scalings from Eqs. (9) and (8). Densities from the divertor probes are corrected for M=1.

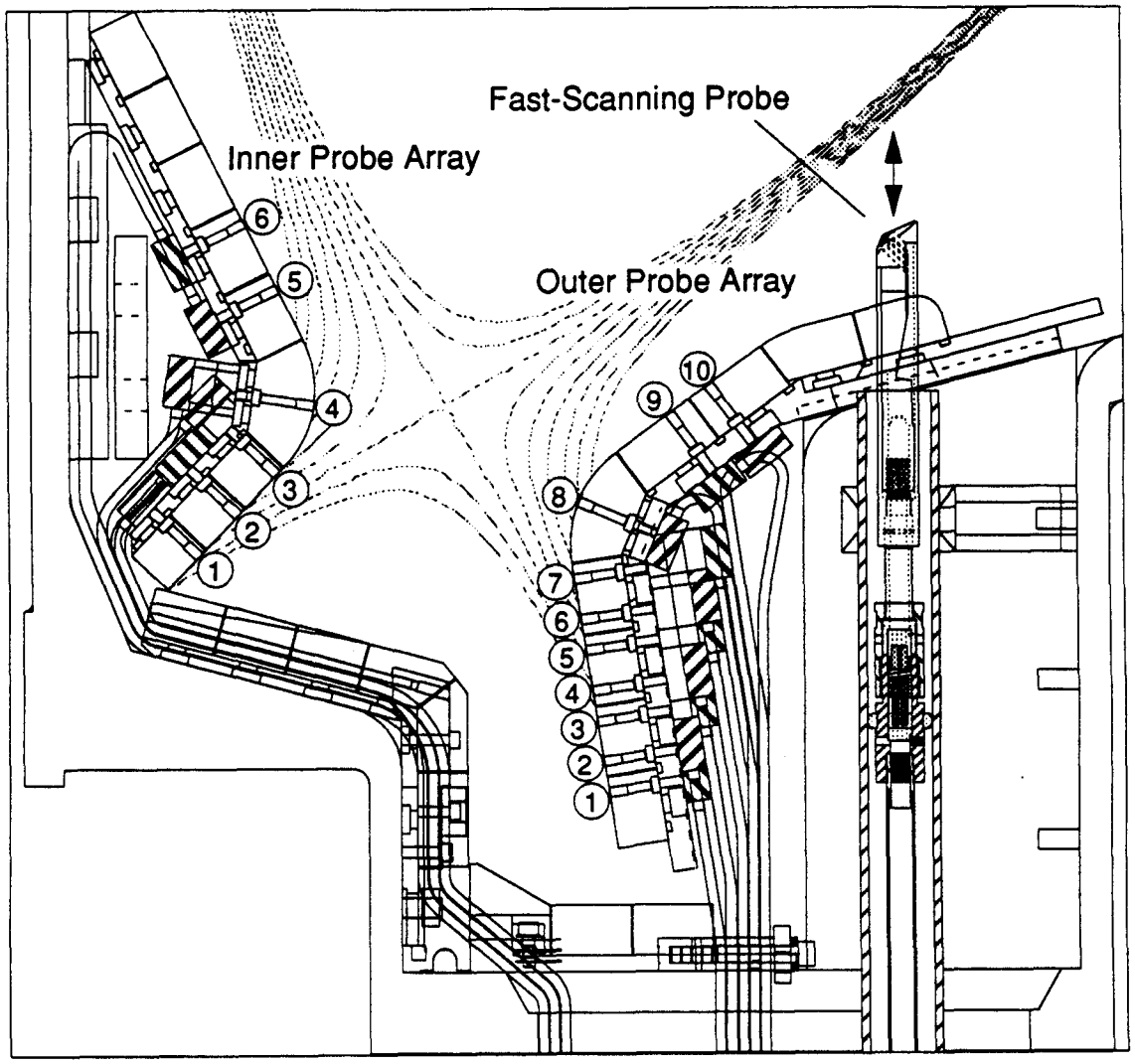
Fast-Scanning Probe
Inner Probe Array
Outer Probe Array
6
5
4
3
2
1
10
9
8
7
6
5
4
3
2
1

Figure 1

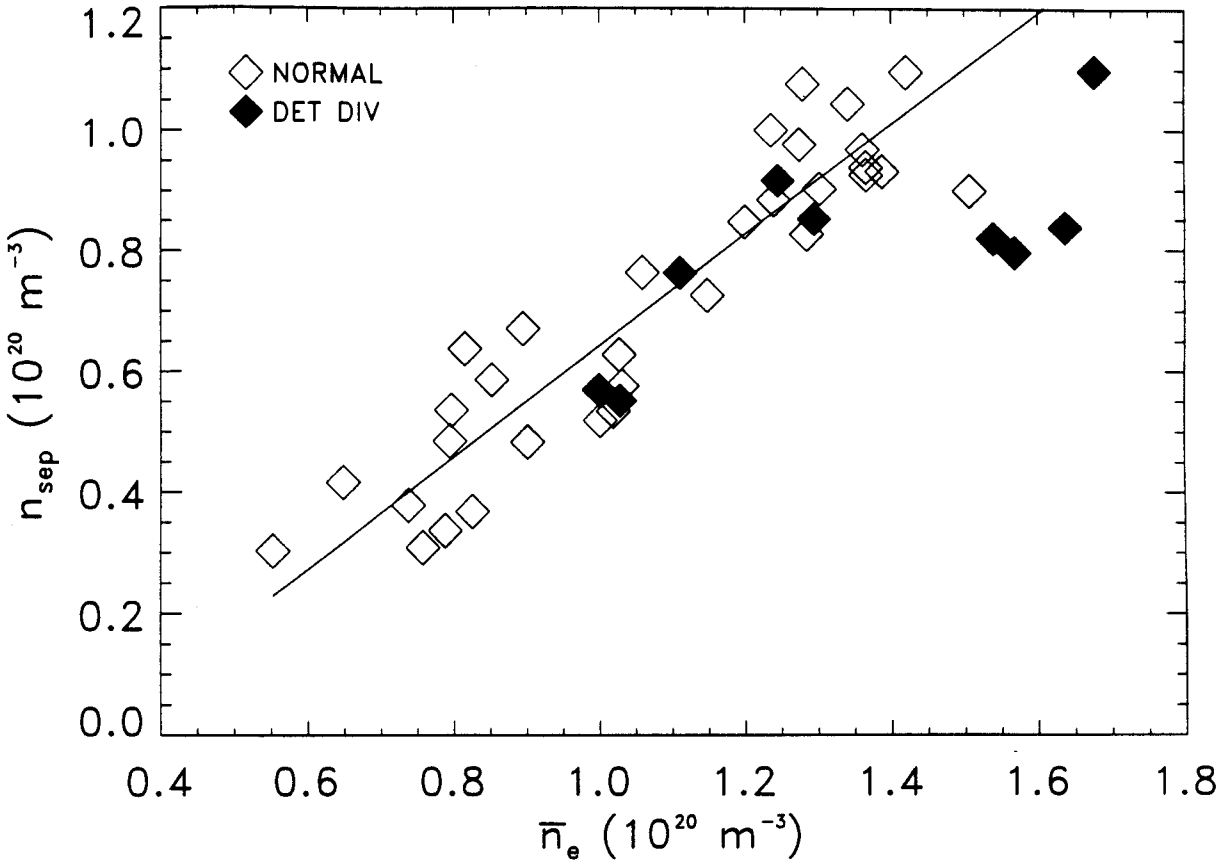
NORMAL
DET DIV
1.2
1.0
0.8
0.6
0.4
0.2
0.0
$n_{sep}$ ($10^{20}$ $m^{-3}$)
0.4
0.6
0.8
1.0
1.2
1.4
1.6
1.8
$\bar{n}_e$ ($10^{20}$ $m^{-3}$)

Figure 2

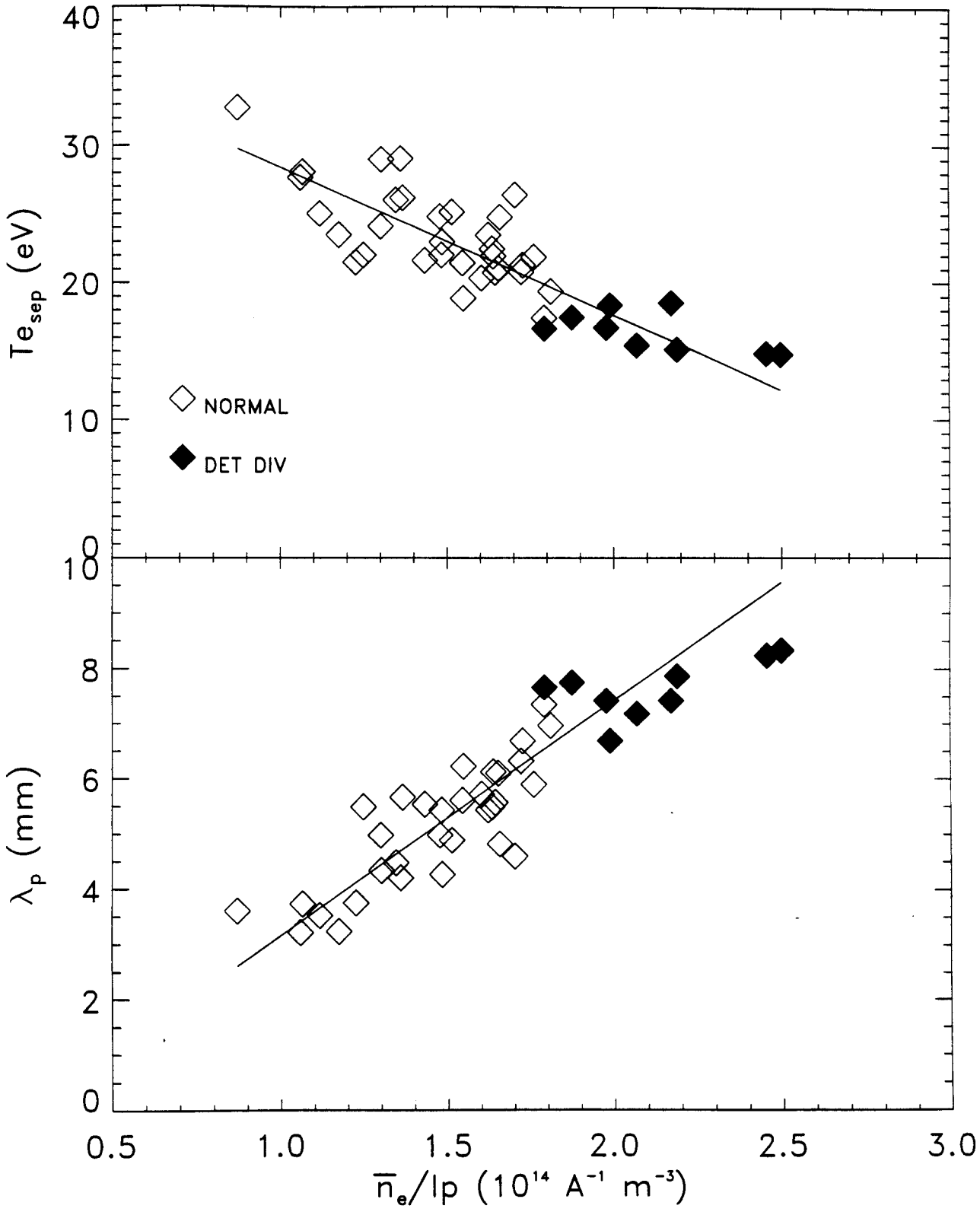
40
30
20
10
0
$Te_{sep}$ (eV)
NORMAL
DET DIV
10
8
6
4
2
0
$\lambda_p$ (mm)
0.5
1.0
1.5
2.0
2.5
3.0
$\overline{n}_e/Ip$ ($10^{14}$ $A^{-1}$ $m^{-3}$)

Figure 3

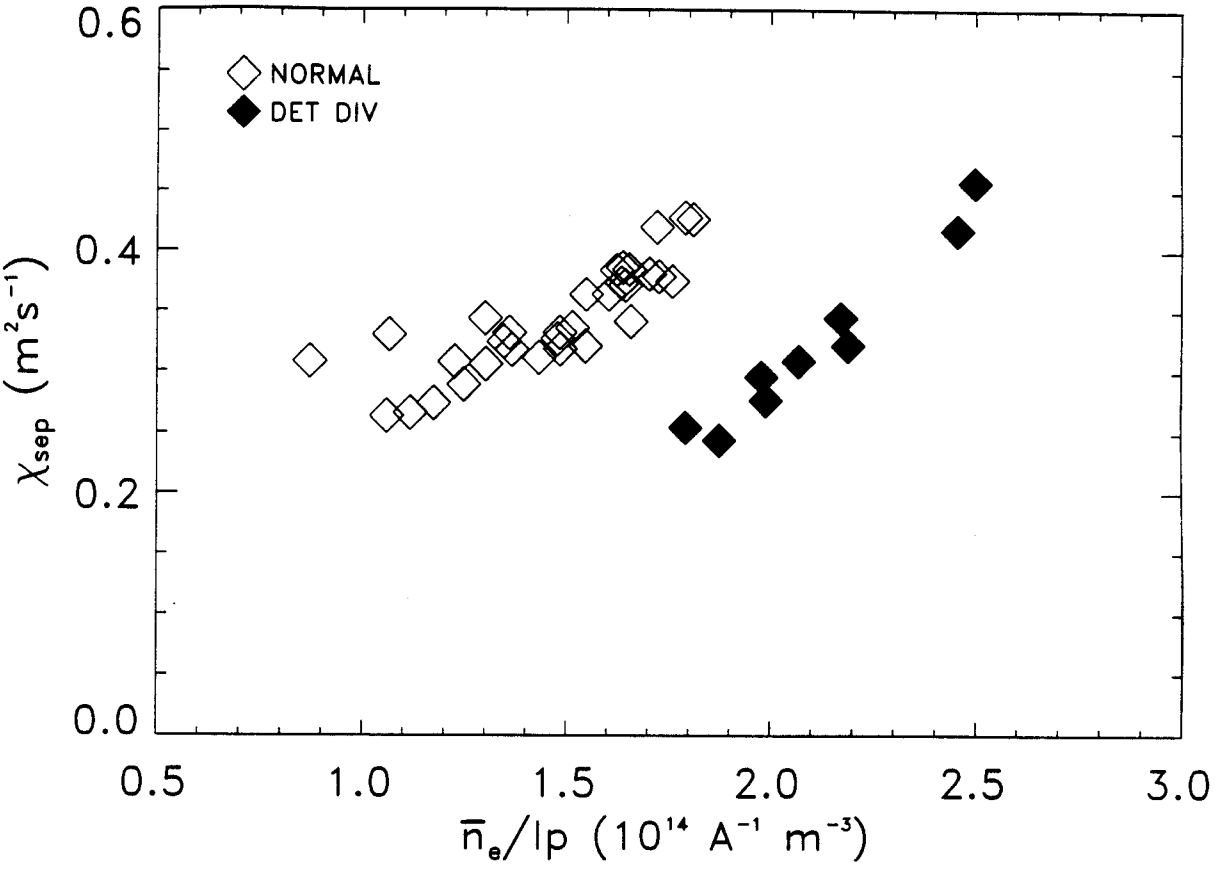
NORMAL
DET DIV
0.6
0.4
0.2
0.0
0.5
1.0
1.5
2.0
2.5
3.0
$\chi_{sep}$ ($m^2s^{-1}$)
$\bar{n}_e/Ip$ ($10^{14}$ $A^{-1}$ $m^{-3}$)

Figure 4

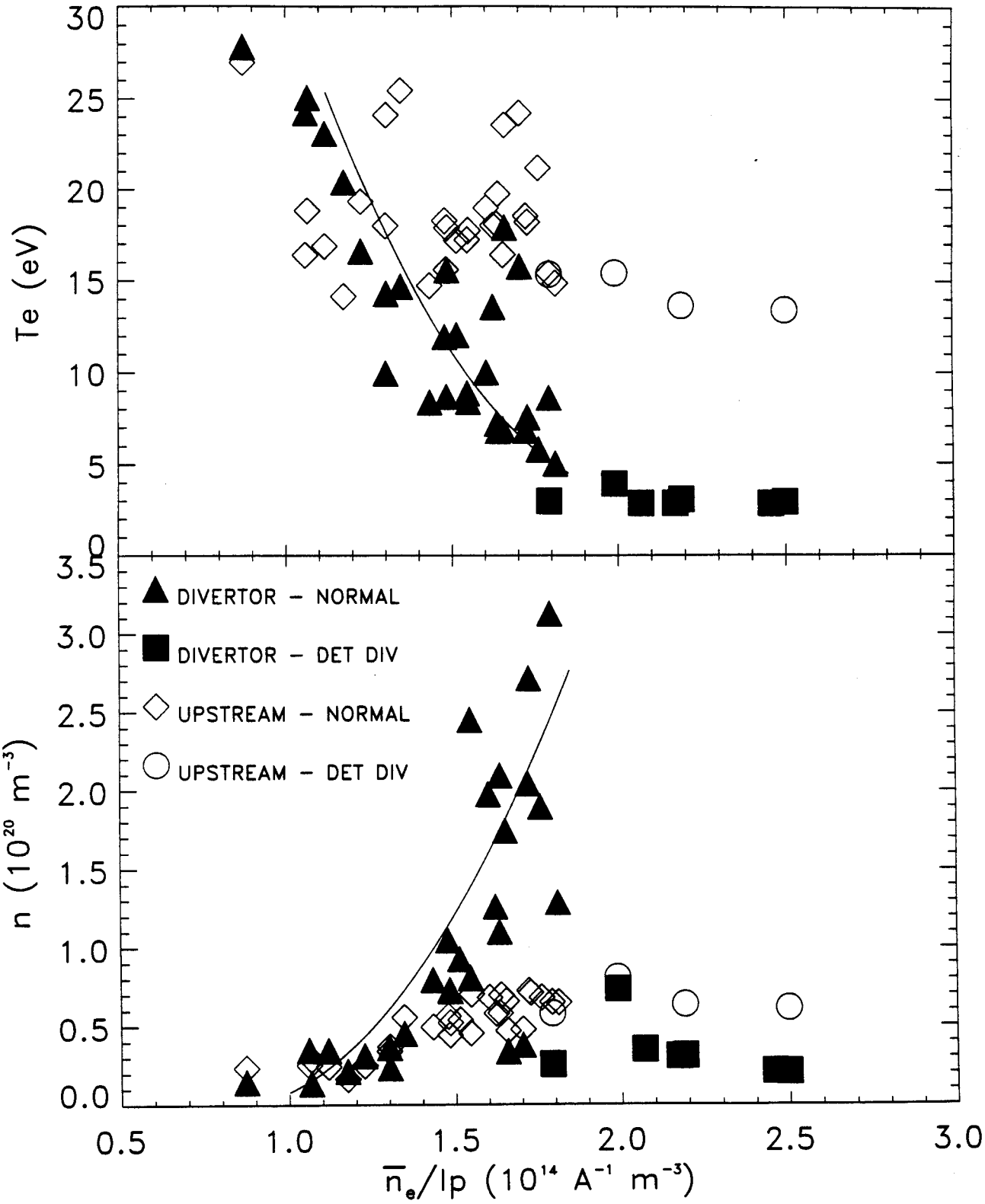
Te (eV)
n ($10^{20}$ m$^{-3}$)
$\overline{n}_e$/Ip ($10^{14}$ A$^{-1}$ m$^{-3}$)
DIVERTOR – NORMAL
DIVERTOR – DET DIV
UPSTREAM – NORMAL
UPSTREAM – DET DIV

Figure 5